INTERNATIONAL JOURNAL FOR NUMERICAL METHODS IN FLUIDS, VOL. 13, 491–505 (1991)

FINITE ELEMENT ANALYSIS OF AXISYMMETRIC FREE JET IMPINGEMENT

GEORGE MEJAK

Department of Mathematics and Mechanics, FNT, University of Ljubljana, Jadranska 19, Ljubljana, Yugoslavia

SUMMARY

A numerical algorithm to determine the impingement of an axisymmetric free jet upon a curved deflector is presented. The problem is considered within the potential flow theory with the allowance of gravity and surface tension effects. The primary dependent variable is the Stokes streamfunction, which is approximated through finite elements using the isoparametric Hermite Zienkiewicz element. To find the correct position of the free boundaries, a trial-and-error method is employed which amounts to solving a boundary value problem (BVP) for the Stokes streamfunction at each iteration step. An efficient method is proposed to solve this BVP. The algorithm to find the correct position of the free boundaries is tested by computing the impingement upon an infinite disc and a hemispherical deflector. To confirm the correctness of the solution, each problem has been solved using several different mesh gradings. A comparison between the Zienkiewicz and the other standard C^0 finite elements is also given.

KEY WORDS Free jet impingement Axisymmetric Finite element

1. INTRODUCTION

In the present paper we shall perform a numerical analysis of a steady axisymmetric potential flow which, after exiting a duct, impinges upon a curved deflector. Since the position of the deflected jet is unknown in advance, we are dealing with a free boundary value problem (FBVP). The problem under consideration has two free surfaces; one emanates from the deflector tip and constitutes the so-called outer free surface; the other emanates from the end of the duct and constitutes the inner surface. It is the presence of two free surfaces that makes our problem particularly difficult. We remark that as a rule even free surface problems with one unknown boundary are anything but easy, especially if the position of the unknown boundary is correlated with another flow characteristic such as the discharge coefficient in flows over a weir or in spillway problems. As far as the author knows, there are no existence as well as uniqueness results for impingement problems with two free surfaces. However, it has recently been shown[1] that by using variational techniques, proponents of which are Alt, Caffarelli and Friedman, one can prove existence and uniqueness for the problem of impingement upon an infinite deflector. For a survey of a large class of different FBVPs together with pertinent numerical methods we refer to References 2–5.

Since we are dealing with axisymmetric potential flow, we can formulate the problem either in terms of the potential function or in terms of the Stokes streamfunction. The decision as to which one to choose depends largely on which numerical method we would like to employ. It is known that for the method based on the variational principle the streamfunction formulation is

0271–2091/91/140491–15$07.50 *Received August 1990*

preferable (see e.g. Reference 6). On the other hand, it is deemed that for a trial-and-error method the potential function formulation is the only reasonable one (see e.g. Reference 7). This belief is based on the fact that the continuity equation in terms of the potential function corresponds to the Laplace equation in cylindrical co-ordinates. What makes this fact pervasive is that the equation rot $\mathbf{v}=0$ in terms of the Stokes streamfunction Ψ corresponds to a singular equation

$$\Psi_{,rr}+\Psi_{,zz}-\frac{1}{r}\Psi_{,r}=0. \tag{1}$$

For plane flows there is of course no distinction between the two formulations and consequently both have been implemented in the numerical analysis of plane free surface flow problems (see e.g. References 8–11). In contrast, in three-dimensional problems there are no such possibilities and one has to use the velocity potential as the primary dependent variable (see e.g. Reference 12). We note that the adjustment of the free surface in the streamfunction formulation is somewhat easier than in the potential function formulation. This is why it would be preferable if we could also economically apply the streamfunction formulation in axisymmetric problems. We show now that this is indeed possible.

First we note that a very simple transformation $\Psi=(\sqrt{r})u$ transforms (1) into

$$u_{,rr}+u_{,zz}-\frac{3}{4r^2}u=0. \tag{2}$$

The resulting equation is still singular, but as was shown by the author,[13] its singularity does not prevent one from using the standard Galerkin method. What is also important is that the transformed problem is a symmetric problem and thus admits a rather economical solution method.

In what follows we shall treat our axisymmetric free surface problem in terms of the Stokes streamfunction. To determine the free surfaces, we apply a trial-and-error method based on the solution of the transformed problem (2). To solve the transformed problem on the assumed domain, we shall employ the finite element method with the isoparametric Hermite Zienkiewicz triangle. Regarding the choice of FEM, we would not like to enter into discussion of which particular method among BIM, FD, FEM and finite volume is preferable. We rather support the opinion that each of them has its merits and thus deserves to be included and evolved in any numerical package of great versatility. We hope that for all who share our opinion the presentation of the rarely used isoparametric Zienkiewicz triangle will be of some interest.

2. STATEMENT OF THE PROBLEM

Since the flow is assumed to be axisymmetric, it suffices to consider only the upper half of the meridian plane. With reference to Figure 1, an axisymmetric deflector BC is placed against a duct GG′. Fluid exiting from the duct impinges upon the deflector, curves back and thus forms a plume CDEF. The problem consists of locating the free surfaces CD and EFG together with other flow characteristics such as the drag on the deflector BC and the pressure distribution along the deflector.

The fluid is assumed to be incompressible and inviscid. We further restrict our considerations to steady irrotational flow. Since we consider an axisymmetric problem, gravity is allowed to act only in the axial direction. In addition to gravity we allow also surface tension effects. We remark that it is known (see e.g. References 14–16) that the potential model is acceptable in impingement problems where inertia and surface tension forces are dominant over viscous forces.

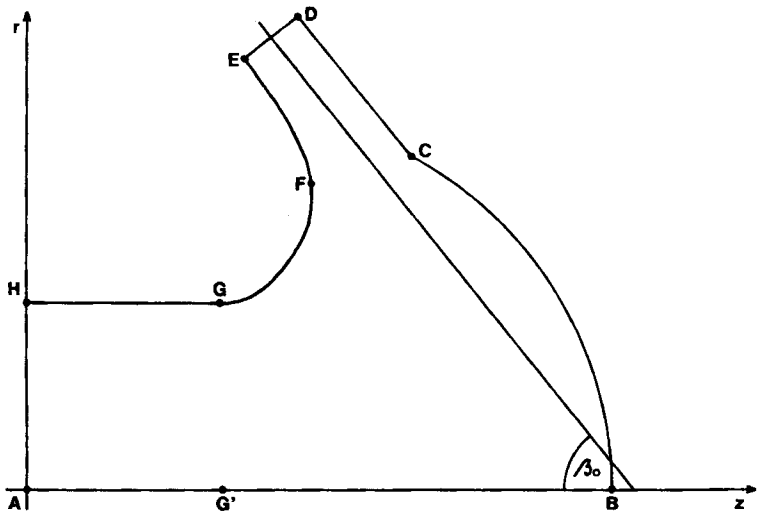

Figure 1. Scheme of the flow domain

In our paper we adopt the notation of capital letters R, Z, V and Ψ for quantities with physical dimensions and respective small letters for their dimensionless values. Here R and Z stand for the radial and axial co-ordinates respectively, V is the magnitude of the velocity vector and Ψ is the volumetric flow rate. Their corresponding dimensionless values are obtained in the following manner. Let R_0 be the characteristic length, V_0 the characteristic speed and let Q denotes the flux. Then we let $r=R/R_0$, $z=Z/R_0$, $v=V/V_0$, and $\psi=2\pi\Psi/Q$. For the characteristic length we take the radius of the duct $\overline{AH}$ and for the characteristic speed the average speed V_0 at the inlet AH. Thus we have $Q=\pi V_0 R_0^2$.

As already mentioned, we formulate the problem in terms of the Stokes streamfunction ψ. By the introduction of the streamfunction the continuity equation is satisfied and thus it remains to solve the equation of irrotationality

$$\psi_{,rr}+\psi_{,zz}-\frac{1}{r}\psi_{,r}=0, \tag{3}$$

together with the appropriate boundary conditions. Since the axis of symmetry AB, the deflector BC, the duct HG and the free surfaces CD and EG are streamlines, we have

$$\psi=0 \quad \text{along AB–BC–CD,} \tag{4}$$

$$\psi=1 \quad \text{along HG–GE.} \tag{5}$$

Along AH we may impose either a Dirichlet or a Neumann condition. If we specify a uniform inlet flow, we have

$$\frac{\partial\psi}{\partial\mathbf{n}}=0 \quad \text{along AH,} \tag{6}$$

where $\mathbf{n}$ is the unit outward normal vector. Alternatively we can specify a given velocity distribution along AH by imposing adequate Dirichlet values for ψ. Here we remark that it might be just as possible to consider the problem with a zero length of the duct HG.

At the outlet the situation is a little more complicated. Here we cannot impose, but only assume, the velocity distribution. It is common practice to assume a uniform flow along DE. In particular we employ

$$\frac{\partial \psi}{\partial \mathbf{n}} = 0 \quad \text{along DE}, \tag{7}$$

or alternatively a corresponding Dirichlet value for ψ along DE.

If the flow domain were known, then we would have already specified all necessary boundary conditions. However, we are dealing with a free boundary problem and thus the unknown location of the free boundaries has to be somewhat compensated by additional boundary conditions along the free boundaries. In flow problems we usually have a constant pressure along free streamlines, which allows one to specify through the Bernoulli equation Neumann boundary conditions for ψ. In particular we have

$$\frac{1}{R}\left|\frac{\partial \Psi}{\partial \mathbf{n}}\right| = V \tag{8}$$

along a streamline at a point with co-ordinates (R, Z) and

$$\tfrac{1}{2}V_a^2 + P_a/\rho - gZ_a = \tfrac{1}{2}V_b^2 + P_b/\rho - gZ_b,$$

where values with subscript 'a' correspond to a point at the inlet and values with subscript 'b' correspond to a point at the free surface. We assume that the speed V_a equals the characteristic speed V_0 and that $Z_a = 0$.

At the free surface the pressure is given by

$$P_b = P_{am} + \sigma\left(\frac{1}{R_1} + \frac{1}{R_2}\right), \tag{9}$$

where P_{am} is the ambient pressure, σ is the coefficient of surface tension (see e.g. Reference 17) and R_1 and R_2 are the two principal radii of curvature. For a parametric positive-oriented dimensionless representation of the free boundary $r = r(t)$, $z = z(t)$ the principal radii are expressed in the following way:

$$\frac{1}{R_1} = \frac{\ddot{r}\dot{z} - \dot{r}\ddot{z}}{R_0(\dot{z}^2 + \dot{r}^2)^{3/2}} = \frac{r_1}{R_0},$$

$$\frac{1}{R_2} = \frac{-\dot{z}}{R_0 r(\dot{z}^2 + \dot{r}^2)^{1/2}} = \frac{r_2}{R_0}.$$

After some manipulations we derive for the speed v_b at the free boundary

$$v_b^2 = 1 + P_r - \frac{2}{We}\left(\frac{1}{r_1} + \frac{1}{r_2}\right) + \frac{2}{Fr} z_b, \tag{10}$$

where $P_r = (P_a - P_{am})/\tfrac{1}{2}\rho V_0^2$ is the pressure ratio, $We = \rho V_0^2 R_0/\sigma$ is the Weber number and $Fr = V_0^2/gR_0$ is the Froude number. The above formula differs from a similar formula in Reference 15 in which the explicit reference to the pressure ratio is compensated by placing the reference point with the subscript 'a' at the end of the duct.

Thus from the boundary conditions (4) and (5) and the dimensionless form of (8) we get the following additional boundary conditions along the free surfaces:

$$\frac{\partial \psi}{\partial \mathbf{n}} = -2rv \quad \text{along CD,} \tag{11}$$

$$\frac{\partial \psi}{\partial \mathbf{n}} = 2rv \qquad \text{along EG,} \tag{12}$$

where the speed v is calculated from (10).

3. FREE SURFACE ADJUSTMENT

As mentioned in the introduction, we are employing in our paper a trial-and-error method. We note that for many free surface problems there exists a much better method. This is especially true for problems for which there exists a transformation into an equivalent variational inequality problem. Usually such transformations exist for plane problems, where one can use the hodograph transformation (see e.g. Reference 18). We remark that for certain axially symmetric free surface problems there exists also the variational inequality formulation (see e.g. Reference 19). For other possible methods see e.g. References 20–23. It is worth making the observation that since free surface flow problems are non-linear problems, any numerical method involves some sort of iteration.

The trial-and-error method is a very simple one. We begin with an assumed location of the free boundaries and then start the iteration in the following manner. Since we have two boundary conditions on each free boundary, at the first step we use one of them together with the given boundary conditions on the fixed part of the boundary to solve the BVP for the governing equation. At the second step we use the remaining boundary conditions on the free boundaries to adjust the free boundaries. If the adjustment is sufficiently small, the iteration is terminated; otherwise we return to the first step. We remark that for some simple FBVPs the trial-and-error method leads to existence results (see e.g. Reference 24).

In this paper, at the first step we use the Neumann boundary conditions (11) and (12) together with the boundary conditions on the fixed part of the boundary. After obtaining the solution of the BVP on the assumed domain, we determine the free boundary adjustments from the Dirichlet conditions

$$\psi = 0 \quad \text{along CD,} \qquad \psi = 1 \quad \text{along EF} \tag{13}$$

through the formula

$$\delta s = \frac{\psi_0 - \psi}{\partial \psi / \partial \mathbf{n}}. \tag{14}$$

Here δs stands for the shift in the normal direction on the free boundary, $\psi_0 = 0$ on CD and $\psi_0 = 1$ on EG. We might instead of the linear approximation (14) use a quadratic one. This is possible since the intrinsic equation of motion $\partial v / \partial \mathbf{n} = -\kappa v$, where v stands for the speed and κ for the curvature of a streamline in the meridian plane (see. e.g. Reference 25, Section 20), and (11) and (12) yield

$$\frac{\partial^2 \psi}{\partial \mathbf{n}^2} = \frac{\partial \psi}{\partial \mathbf{n}} \left(\frac{n_r}{r} - \kappa \right).$$

We note that the quadratic approximation is justifiable only then when the assumed free boundary is almost a streamline. However, we have found the linear approximation (14)

satisfactory enough and thus we here present results obtained only on the basis of the linear approximation.

In the plume region CDEF we have two free surfaces and consequently one might expect some special treatment as in Reference 15. However, in our numerical experiments we found that simultaneous adjustment of both free boundaries at each iterative step works very satisfactorily. In fact, in the case of alternating adjustments we observed oscillation behaviour. At this point we would like to emphasize that the above-mentioned method sometimes converged to physically unacceptable solutions, especially if the initial approximation of the free boundaries was poor. This physical unacceptance was demonstrated in an unacceptable shape of the outer free boundary and also in a pressure discontinuity at the tip of the deflector. We refer to the pressure discontinuity as the difference between the pressure imposed by (9) and the pressure calculated from the FEM solution. To redeem the situation, we employed a rotation of the plume region—a similar algorithm to that in Reference 16. In the case when the calculated pressure at C was greater than it should be we rotated the plume about C in a clockwise direction. For too low a pressure the plume was rotated in the opposite direction. As our numerical experiments showed, the improved iteration converges to a physically acceptable solution. We note that at each step of the iteration we perform either a rotation or a free surface adjustment. Of course, when the adjustment starts to redeem the pressure discrepancy we may dispense with the rotation. As we shall see later, use of the Zienkiewicz triangle element at this point enables us to impose the pressure continuity as the constraint. The exact amount of a rotation is of an empirical nature but can be programmed without difficulty.

Since the adjustment of the free boundaries also shifts the points D and E, we have to redefine the boundary DE too. In order to justify the boundary condition (7), we take for the new curve DE a cubic curve orthogonal at its ends the free boundaries.

4. SOLUTION OF THE GOVERNING EQUATION

In the preceding section we found that at each iteration step we have to solve the boundary value problem

$$\begin{aligned} \psi_{,rr}+\psi_{,zz}-\frac{1}{r}\psi_{,r}&=0 \quad \text{in } \Omega,\\ \psi&=g_1 \quad \text{on } \Gamma_1,\\ \frac{\partial\psi}{\partial\mathbf{n}}&=g_2 \quad \text{on } \Gamma_2, \end{aligned} \tag{15}$$

where Ω is the flow domain, Γ_1 is the union of the arcs $AB \cup BC \cup GH$ and Γ_2 is the union $CD \cup DE \cup EG \cup HA$. The functions g_1 and g_2 are defined by

$$g_1(r,z)=\begin{cases} 0 & \text{along AB}\cup\text{BC},\\ 1 & \text{along HG}, \end{cases}$$

$$g_2(r,z)=\begin{cases} 0 & \text{along DE}\cup\text{HA},\\ -2r\sqrt{\left[1+P_r-\dfrac{2}{We}\left(\dfrac{1}{r_1}+\dfrac{1}{r_2}\right)+\dfrac{2}{Fr}z\right]} & \text{along CD},\\ 2r\sqrt{\left[1+P_r-\dfrac{2}{We}\left(\dfrac{1}{r_1}+\dfrac{1}{r_2}\right)+\dfrac{2}{Fr}z\right]} & \text{along EG}. \end{cases}$$

Since the BVP (15) has to be solved many times for different partial domains, its solution method must be a very economical one. In this paper we use the FEM, although it is quite possible that some other method might be even more economical. We note first that (15) after the discretization leads to an asymmetric system. However, a very simple transformation $\psi=(\sqrt{r})u$ transforms (15) into

$$\begin{aligned} u_{,rr}+u_{,zz}-\tfrac{3}{4}r^{-2}u&=0 \quad \text{in } \Omega,\\ (\sqrt{r})u&=g_1 \quad \text{on } \Gamma_1,\\ \tfrac{1}{2}r^{-1}n_r u+\frac{\partial u}{\partial \mathbf{n}}&=\frac{g_2}{\sqrt{r}} \quad \text{on } \Gamma_2, \end{aligned} \tag{16}$$

which obviously leads to a symmetric system. Of course, the transformation does not resolve the question of singularity; it even introduces an additional singular term into the boundary condition on Γ_2. However, it was shown by the author[13] that the singularity of the transformed problem does not prevent one using the standard Galerkin procedure. In fact, it was shown that the corresponding linear forms

$$a(u,w)=\int_\Omega\left(\frac{\partial u}{\partial r}\frac{\partial w}{\partial r}+\frac{\partial u}{\partial z}\frac{\partial w}{\partial z}+\tfrac{3}{4}r^{-2}uw\right)\mathrm{d}r\mathrm{d}z,$$

$$b(u,w)=\tfrac{1}{2}\int_{\Gamma_2} r^{-1}n_r uw\,\mathrm{d}s$$

are well defined and bounded on $H^1_{AB}(\Omega)=\{w: w\in H^1(\Omega) \text{ and } \gamma w|_{AB}=0\}$. Here we have adopted the standard notation $H^1(\Omega)$ for the Sobolev space and γ for the trace operator (see e.g. Reference 26). It follows from the boundedness of the forms that BVP (16) admits an equivalent variational problem. We note that there is no need to use any special elements near the axis since the boundary condition $g_1=0$ along the axis already handles the singularity in (16). This is to be compared with another approach where the solution ψ is obtained by solving the variational problem

$$\int_\Omega \frac{1}{r}\left(\frac{\partial \psi}{\partial r}\frac{\partial w}{\partial r}+\frac{\partial \psi}{\partial z}\frac{\partial w}{\partial z}\right)\mathrm{d}r\,\mathrm{d}z=\int_{\Gamma_2}\frac{1}{r}g_2 w\,\mathrm{d}s$$

for all admissible functions w; but here, since the flow domain Ω also includes the symmetry axis, one must pay attention to the singular term r^{-1} in the area integral.

At each individual step of the iteration we have to solve the BVP (16) on a domain which is different from the domain at the previous step. This in principle involves the generation of a new mesh and assemblage of the global matrix at each iterative step. Of course there is no need to change the mesh over the whole domain. It suffices to divide the mesh into fixed and moving parts. This division after the first iteration step reduces the assemblage procedure only on elements from the moving part. In the determination of the fixed part we must take care that elements from the moving part during the iteration do not become too distorted or even overlap the fixed part.

Needless to say, the mesh generation must be a universal one, i.e. it must work for almost all possible shapes of deflector. For this purpose we have found the following procedure especially convenient. We define an L-shaped domain as the reference domain. Its dimensions are determined through the geometric parameters of the flow problem, i.e. the radius and length of the duct, the jet-to-deflector clearance and the length of the deflector and the plume. Then we generate a triangular mesh on the reference domain and conformally map the reference domain

together with its mesh onto the flow domain. To perform this mapping, we have to solve two Dirichlet BVPs for the Laplacian for r- and z-co-ordinates. We solve these BVPs with the FEM using linear elements. Employing these elements at this stage and the later use of the Zienkiewicz elements allow us to apply the same scheme for the mesh of the flow domain. It is worth noting that we have to assemble the stiffness matrix of the conformal mapping problem only once. All that we have to do at each later step is to perform two back-substitutions. The fixed and moving parts of the mesh are first determined on the reference domain and then mapped onto the flow domain. We note that for problems with abrupt separation at the deflector tip the conformal mapping of the L-shaped domain sometimes produces overlapping elements in the vicinity of the deflector tip. To overcome this problem, we relocate the nodes in the neighbourhood of the deflector tip. Since the location of the boundary and middle nodes is correct, it is easy to rectify the grid in the neighbourhood of the deflector tip.

5. ISOPARAMETRIC HERMITE ELEMENT

There are at least two reasons for employing Hermite elements. The first is related to the storage requirements and the second to the need to accurately calculate the pressure distribution along the deflector. We use isoparametric elements to fit the curved free boundaries accurately.

As is known, the concentration of degrees of freedom at an individual node reduces the storage requirements for the global stiffness matrix. The Zienkiewicz triangle has three nodes and at each node three degrees of freedom, i.e. the value of a function and the values of its two partial derivatives (see e.g. Reference 27). The corresponding basis functions $\hat{\Psi}^0_k$, $\hat{\Psi}^1_{k1}$ and $\hat{\Psi}^1_{k2}$ for the master element in the (ξ, η)-plane have the following properties:

$$\begin{aligned}
&\hat{\Psi}^0_k(\hat{a}_i)=\delta_{ki}, \qquad \frac{\partial}{\partial\xi}\hat{\Psi}^0_k(\hat{a}_i)=\frac{\partial}{\partial\eta}\hat{\Psi}^0_k(\hat{a}_i)=0,\\
&\hat{\Psi}^1_{k1}(\hat{a}_i)=0, \qquad \frac{\partial}{\partial\xi}\hat{\Psi}^1_{k1}(\hat{a}_i)=\delta_{ki}, \qquad \frac{\partial}{\partial\eta}\hat{\Psi}^1_{k1}(\hat{a}_i)=0, \qquad (17)\\
&\hat{\Psi}^1_{k2}(\hat{a}_i)=0, \qquad \frac{\partial}{\partial\xi}\hat{\Psi}^1_{k2}(\hat{a}_i)=0, \qquad \frac{\partial}{\partial\eta}\hat{\Psi}^1_{k2}(\hat{a}_i)=\delta_{ki}.
\end{aligned}$$

Here i and k run over the set $\{1, 2, 3\}$ and $\hat{a}_i$ denote the vertices of the master element.

The master element $\hat{\Omega}$ is transformed to an isoparametric element Ω_e in the computational space through a linear combination of the basis functions of the master element. Since we have nine basis functions, we have nine coefficients at our disposal. In particular, it follows from (17) that the transformation.

$$F:(\xi,\eta)\mapsto x=a_k\hat{\Psi}^0_k(\xi,\eta)+\xi_{k1}\hat{\Psi}^1_{k1}(\xi,\eta)+\xi_{k2}\hat{\Psi}^1_{k2}(\xi,\eta) \qquad (18)$$

maps the master element onto a curved triangle with vertices a_k and sides which are cubic curves and have at the vertices (see Figure 2) tangents t_j, $j=1, 2, \ldots, 6$ such that

$$\begin{aligned}
&t_1=\xi_{11}/s_3, \qquad t_2=\xi_{12}/s_2, \qquad t_3=(\xi_{22}-\xi_{21})/s_1,\\
&t_4=-\xi_{21}/s_3, \qquad t_5=-\xi_{32}/s_2, \qquad t_6=(\xi_{31}-\xi_{32})/s_1.
\end{aligned}$$

Here s_k denotes the length of the side of the curved triangle which lies opposite the vertex a_k. Of course the transformation (18) should be invertible and to this end it suffices to require that the element Ω_e is not too distorted.

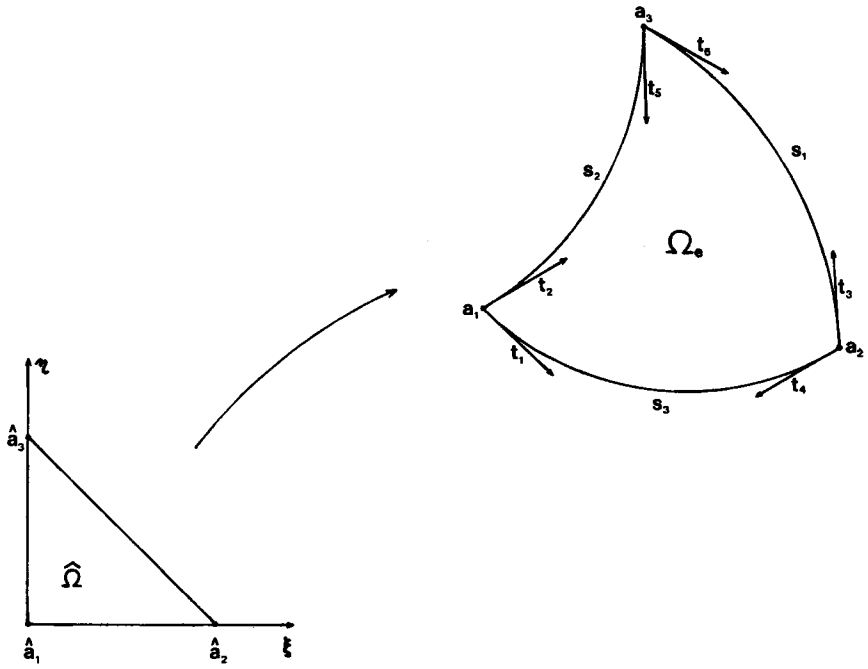

Figure 2. Isoparametric transformation

The basis functions Ψ_k^0 and Ψ_{kl}^1 are on Ω_e defined through a composition of the inverse of the isoparametric mapping (18) and the master basis functions:

$$\Psi_k^0(x)=\hat{\Psi}_k^0(F^{-1}(x)) \qquad \Psi_{k1}^1(x)=\hat{\Psi}_{k1}^1(F^{-1}(x)) \qquad \Psi_{k2}^1(x)=\hat{\Psi}_{k2}^1(F^{-1}(x)).$$

It follows from (17) and (18) that the local interpolation operator Π on $C^1(\bar{\Omega}_e)$ is given by

$$\Pi v=\sum_{k=1}^{3}[v(a_k)\Psi_k^0+Dv(a_k)(\xi_{k1}\Psi_{k1}^1+\xi_{k2}\Psi_{k2}^1)],$$

with the local degrees of freedom $a_k\in\mathbb{R}^3$ at the point a_k given by

$$a_k=[v(a_k), Dv(a_k)\xi_{k1}, Dv(a_k)\xi_{k2}]^T. \tag{19}$$

Now, following the standard procedure, we obtain a symmetric algebraic system $\mathbf{K}_e\boldsymbol{a}=\mathbf{f}_e$, where $\mathbf{K}_e$ is the element stiffness 9×9 matrix, $\mathbf{f}_e\in\mathbb{R}^9$ is the element load vector and $\boldsymbol{a}\in\mathbb{R}^9$ is a vector of local degrees of freedom, $\boldsymbol{a}=[a_1^T, a_2^T, a_3^T]^T$. At this point we observe that in order to assemble the element stiffness matrix $\mathbf{K}_e$ into the global one, we need to express the local degrees of freedom a_k in global degrees $\boldsymbol{\beta}=[\boldsymbol{\beta}_1^T, \boldsymbol{\beta}_2^T, \boldsymbol{\beta}_3^T]^T$, where

$$\boldsymbol{\beta}_k=\left[v(a_k), \frac{\partial v}{\partial x_1}(a_k), \frac{\partial v}{\partial x_2}(a_k)\right]^T. \tag{20}$$

It is easy to see that multiplication of the vector $\boldsymbol{a}$ by the matrix $\mathbf{H}$, where

$$\mathbf{H}=\begin{pmatrix}\mathbf{H}_1 & \mathbf{0} & \mathbf{0}\\ \mathbf{0} & \mathbf{H}_2 & \mathbf{0}\\ \mathbf{0} & \mathbf{0} & \mathbf{H}_3\end{pmatrix},$$

$\mathbf{0} \in \mathbb{R}^{3,3}$ and $\mathbf{H}_k$ is a 3×3 matrix

$$\mathbf{H}_k = \begin{pmatrix} 1 & 0 & 0 \\ 0 & \xi_{k1,1} & \xi_{k1,2} \\ 0 & \xi_{k2,1} & \xi_{k2,2} \end{pmatrix},$$

transforms the global degrees of freedom $\boldsymbol{\beta}$ into the local one $\boldsymbol{\alpha}$. Thus we have $\mathbf{K}_e \mathbf{H}_e \boldsymbol{\beta} = \mathbf{f}_e$. However, since the resulting algebraic system is not symmetric, we multiply it from the right by the transpose $\mathbf{H}^T$ and thus the element contribution to the global system is

$$\mathbf{H}_e^T \mathbf{K}_e \mathbf{H}_e \boldsymbol{\beta} = \mathbf{H}_e^T \mathbf{f}_e.$$

In this way we obtained the symmetric algebraic system with the appropriate global degrees of freedom.

It is worth noting that the use of Hermite elements also requires some care while imposing boundary conditions. In particular, at points where the Dirichlet boundary condition is imposed we have to specify not only a boundary value but also a value of the tangential derivative. Since in general tangential derivatives are not partial derivatives, we have to handle the imposed values of the tangential derivatives as constraints. In our FEM implementation we have taken into account these constraints through the use of the Lagrange multipliers. It is known that this may considerably impair the structure of the global matrix. To this end we inserted the equation with the Lagrange multiplier of the kth node into the global matrix next to the three Galerkin equations of the kth node. Of course, this involves some additional rearrangements, but as we have found, these paid off. We note also that at corner nodes with the Dirichlet boundary condition on both sides we have two directional derivatives, from which we can readily express both partial derivatives, and thus at such points there is no need to use Lagrange multipliers.

As a final remark concerning the use of the Zienkiewicz Hermite triangle we would like to say something about the enumeration of the mesh modes. It is well known (see e.g. Reference 28) that the efficiency of the Cuthill–Mckee ordering algorithms improves with the number of interior and side nodes. Thus it is not surprising, as we have found, that the natural ordering, column by column in the horizontal part of the L-domain and row by row in the vertical part, gives much better results. We note also that the Zienkiewicz element can be fairly easily added to an existing FEM package. This is further enhanced by the fact that the Zienkiewicz element requires the same mesh discretization as the linear triangular element does.

6. NUMERICAL RESULTS

In this section we present numerical results for two axisymmetric free jet problems. For the test problem we took impingement upon an infinite disc and for the problem to show the applicability of our FEM code we chose impingement upon a hemispherical deflector.

As recognized, there is no known analytical solution of axisymmetric free jet impingement problems. However, for the problem of impingement upon an infinite disc a theoretical value of the drag is known, namely π. In addition, this problem is relatively well represented in the literature, which is why we chose it as the test problem. Unfortunately, only Schach[29] gives the drag in his calculation, while Labus and DeWitt[14] and Obee and DeWitt[15] give only the graph of the calculated free surface. In Table I we present our results for different boundary conditions at the outlet as well different mesh gradings. In all presented examples the iteration converged and terminated when the maximal error of computed values of the streamfunction along the free boundary was less than 10^{-5}. We note that the comparison of the calculated drag with the exact

value π is somewhat hindered by the fact that we actually calculated the impingement upon a finite disc of radius $r=4{\cdot}5$. However, the convergence and excellent agreement of the results for different meshes and outlet boundary conditions (see Table I) confirm that we found the 'correct' solution.

In the table we refer to the storage requirement as the number of stored entries of the global stiffness matrix for the skyline storage schema (see e.g. Reference 30). The pressures in the table were calculated at the tip of the disc. Matrix calculations were performed in double-precision arithmetic, while for all other calculations we used single precision. All calculations on a relatively coarse mesh with a storage requirement below 8191 entries could be performed on a personal computer. The restriction up to 8191 entries is intimately correlated with the PC architecture, which allows a COMMON block only up to 64K. Nevertheless, with a PC it is possible to provide a larger computer with a fairly good initial approximation of the free boundaries. For calculations with a storage requirement above 8191 entries we used a VAX computer, model 750.

We solved the same problem on a PC using linear, quadratic and cubic triangular elements and bilinear and biquadratic quadrilateral elements. Convergence of almost the same order was achieved for all these elements (see Table II) and one could possibly conclude that it is sufficient to

Table I. Impingement upon an infinite disc; $P_r=0$, $We=Fr=\infty$

Nodes	Elements	Storage	Outlet BC	Drag	Pressure
146	220	8157	Neumann	3·10295	0·00055
213	324	11877	Dirichlet	3·10100	0·00057
213	324	11835	Neumann	3·10129	0·00061
306	478	19617	Dirichlet	3·10309	0·00055
306	478	19575	Neumann	3·10330	0·00060

Table II. Convergence in terms of the maximal error times 10^5 of the streamfunction along the free boundary for free jet impingement upon an infinite disc using different isoparametric finite elements: T1 = linear, T2 = quadratic and T3 = cubic triangular elements; Q1 = bilinear and Q2 = biquadratic quadrilateral elements; Z = Zienkiewicz element

Iteration	T1	T2	T3	Q1	Q2	Z
1	23476	51432	51310	50361	50972	25635
2	7868	9617	9676	9203	8731	8863
3	2975	1825	3923	3994	3537	3400
4	1121	1485	1509	1653	1381	1344
5	438	572	578	673	530	504
6	169	218	221	227	202	189
7	65	83	84	112	77	63
8	25	32	32	45	29	27
9	9	12	12	18	11	10
10	4	5	5	7	4	4
11	1	2	2	3	2	1
12	0	1	0	1	0	0
Drag	2·08816	2·91150	3·08235	1·73021	3·08440	3·10400
Nodes	146	327	271	97	327	146

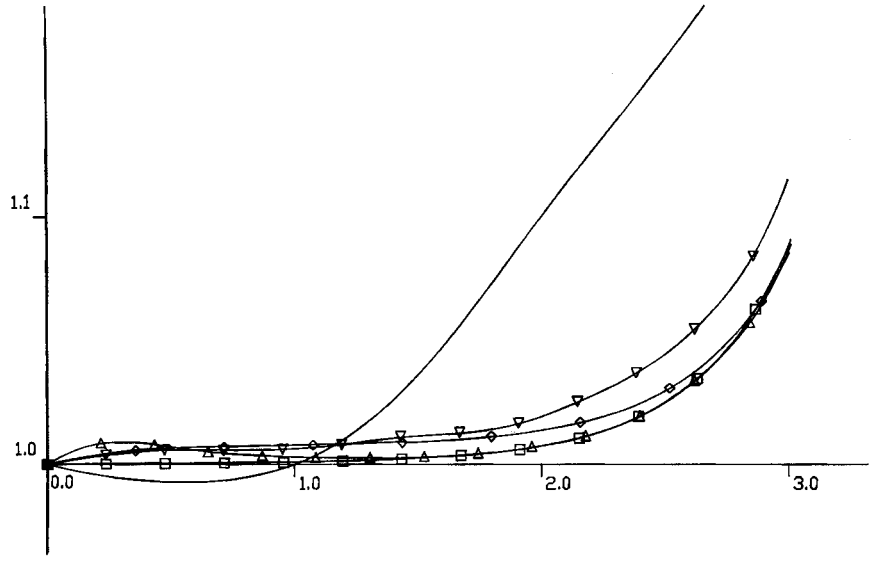

Figure 3. Comparison of the positions of the free boundary for impingement upon an infinite disc for different finite elements. The disc is placed at $z=4{\cdot}0$ and, to emphasize the difference, the r-co-ordinates of the data are multiplied by 10. Special symbols □, ▽, △ and ◇ stand for nodal points of the solution obtained by using the Zienkiewicz, T1, T3 and Q1 elements respectively. The curve without any special symbols is an initial approximation of the free boundary

use linear elements. However, comparison of the computed values of the drag with the theoretical value and, moreover comparison of the imposed values of the normal derivatives with the computed normal derivatives of the solution along the free boundary revealed that the Zienkiewicz element gives the most reliable results. Comparing plots of the free boundary, we have found in this particular example that T2, Q2 and Zienkiewicz elements give almost the same position of the free boundary. The difference between this position and the positions obtained by using T1, T3 and Q1 elements is presented in Figure 3.

We now proceed to the second example. Actually, in the development of our programme we proceeded with the calculation of impingement upon an elliptical deflector, a problem which was initiated by Schnurr *et al.*[31] Since we later found that impingement upon a hemispherical deflector demanded much more, we took it as our representative example. This choice was further enhanced by the available comparison with the results from Reference 16.

The geometry of the problem is determined by the following parameters (see Figure 1): the length of the duct $\overline{HG}$ (l), the jet-to-deflector clearance $\overline{G'B}$ (d) and the radius of the sphere (r_d). Since the variation of values of d, r_d, P_r, We and Fr is an objective of the design analysis of the hemispherical deflector and thus beyond the scope of our paper, we here present only the results for $l=2{\cdot}0$, $d=2{\cdot}0$, $r_d=1{\cdot}8$, $P_r=0{\cdot}5$ and $We=Fr=\infty$. We note only that the numerical difficulty of the problem increases with a decrease of r_d. For a similar observation see also Reference 15. In fact, the smallest value of r_d for which we solved the problem of impingement upon the hemispherical deflector was 1·5.

To see whether the calculated solution is the correct one, we compare solutions of the same problem for different mesh sizes. In addition to this we compare the actual deflection angle β_0 with the deflection angle β calculated from the momentum equation. This calculation rests on the assumption of a linear velocity distribution along the outlet and on the assumption that the

calculated drag on the deflector equals the exact value. If these premises are correct, then for the exact position of the free boundaries β_0 should equal β. However, as our numerical experiments showed, a discrepancy between β and β_0 of up to 0·5° is acceptable. We note that the difference $\Delta\beta = \beta - \beta_0$, which could be calculated at each iteration step, is only a measure of how accurate a solution is and that in principle it says nothing about the angle through which the plume should be rotated.

In Table III we present results for the same problem using the Zienkiewicz element on different meshes. The initial approximation was determined in the following way. For the outer free boundary we took a straight line with the assumed deflection angle $\beta_0 = 20°$. The points E and F were then calculated from the continuity equation and the inner free boundary was determined as a rational interpolation $z = z(r)$ through the points E, F and G with a given asymptote. In obtaining the first result in Table III, we started with the initial approximation. After 32 iterations we proceeded with a finer mesh and finally finished with 255 nodes, corresponding to 765 degrees of freedom. The total number of iterations was 42. In the table we also give the maximal difference $\Delta\psi$ along the free streamlines between a required value ψ_0 and a computed value ψ. To check the accuracy of the solution, we repeated the calculations on a rather fine mesh consisting of 586 elements. We present also plots of the finite element mesh with 408 elements and the streamlines of the solution in Figures 4 and 5 respectively.

The calculated value of β_0 is to be compared with the result $\beta_0 = 20{\cdot}3°$ from Reference 16. This result is not particularly close to our value, but as we have found, both analyses give the same qualitative information on the thrust reversal characteristics of the hemispherical deflector. A

Table III. Impingement upon a hemispherical deflector; $r_d = 1{\cdot}8$, $P_r = 0{\cdot}5$, $We = Fr = \infty$

Nodes	Elements	Storage	β_0	$\Delta\beta$	Drag	$\Delta\psi$ inner	$\Delta\psi$ outer
132	198	7527	22·03	0·90	7·49204	0·00041	0·00026
200	303	11247	22·09	0·47	7·50231	0·00007	0·00003
255	408	19761	22·12	0·38	7·49189	0·00012	0·00005
357	586	29982	22·12	0·32	7·49350	0·00013	−0·00005

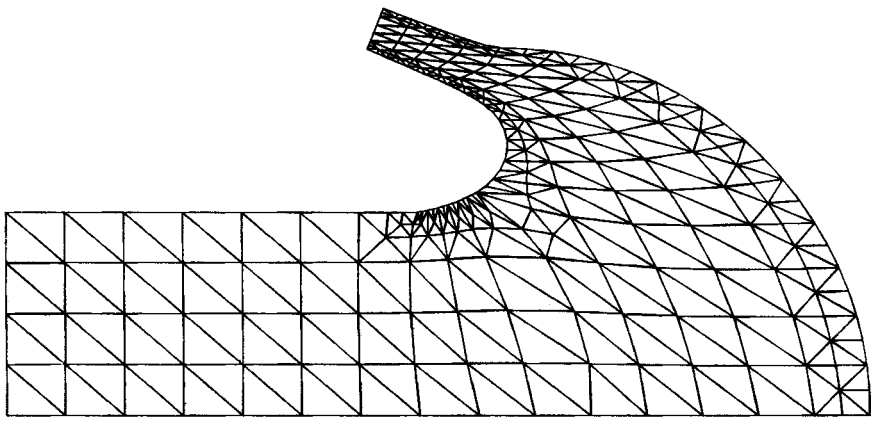

Figure 4. Finite element mesh for free jet impingement upon a hemispherical deflector

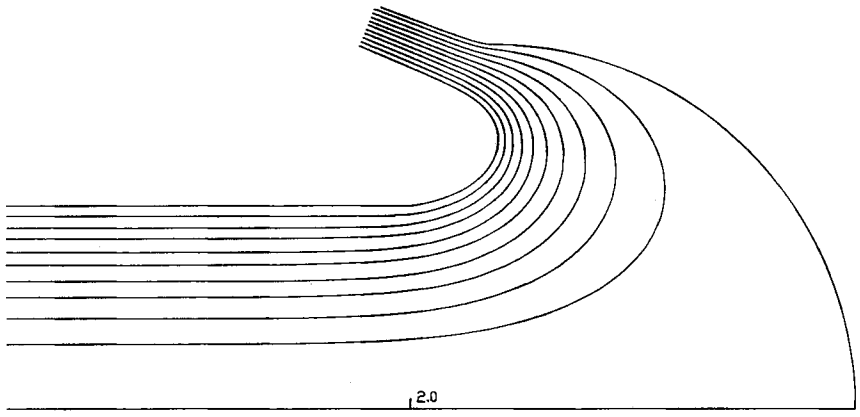

Figure 5. Streamlines of free jet impingement upon a hemispherical deflector

possible reason for the quantitative differences between the two computations is that we have specified the pressure ratio. Moreover, we have also imposed the C^1 smooth fit for the free boundaries.

7. CONCLUSIONS

In this paper we have presented the isoparametric Hermite Zienkiewicz element in calculations of free jet impingement problems. Using this element, we have found the following.

1. Boundaries of the domain are approximated very accurately. Moreover, free boundaries can be approximated by a C^1 smooth curve and one can even impose the smooth fit at points where a free boundary separates from the fixed boundary.
2. Velocities are calculated more accurately than in other standard C^0 finite elements. This allows one to use the momentum equation as the criterion of the correctness of the solution. To have such a criterion is very important, since as we have seen, convergence of the method is not always a guarantee of the correctness of the solution.
3. At certain points on the boundary, in particular at the tip of the deflector and at the lip of the duct, it is possible to directly impose a value of the normal derivative and thus specify the pressure at these points.
4. For the same number of degrees of freedom the half-bandwidth of the global stiffness matrix is considerably smaller than for other standard C^0 finite elements. With this reduction in storage requirement it is possible to obtain relatively satisfactory results by using only a PC.

REFERENCES

1. Chen Xinfu, 'Axially symmetric jets of compressible fluid', *IMA Preprint Series 620*, University of Minnesota, Minneapolis, MN, 1990.
2. J. V. Wehausen, 'Free-surface flows', in R. J. Seeger and G. Temple (eds), *Research Frontiers in Fluid Dynamics*, Wiley, New York, 1965, pp. 534–640.
3. C. Taylor, 'The utilization of the FEM in the solution of some free surface problems', *Proc. 3rd Int. Conf. on Finite Elements in Flow Problems*, Banff, Alberta, 1980, Vol. 1, University of Calgary, 1980, pp. 54–81.
4. R. W. Yeung, 'Numerical methods in free-surface flows', *Ann. Rev. Fluid Mech.*, **14**, 395–442 (1982).
5. J. Crank, *Free and Moving Boundary Problems*, Oxford University Press, Oxford, 1984.

6. J. M. Aitchison, 'The numerical solution of planar and axisymmetric cavitational flow problem', *Comput. Fluids*, **12**, 55–65 (1984).
7. S. T. K. Chan and B. E. Larock, 'Fluid flows for axisymmetric orifices and valves', *J. Hydraul. Div., Proc. ASCE*, **99**, (HY1), 81–97 (1973).
8. S. T. K. Chan, B. E. Larock and L. R. Herrmann, 'Free-surface ideal fluid flows by finite elements', *J. Hydraul. Div., Proc. ASCE*, **99**, (HY6), 959–976 (1973).
9. T. J. Chung, *Finite Element Analysis in Fluid Dynamics*, McGraw-Hill, New York, 1978.
10. L. T. Isaacs, 'Numerical solution for flow under sluice gates', *J. Hydraul. Div., Proc. ASCE*, **103**, (HY5), 473–481 (1977).
11. A. H. D. Cheng, J. A. Ligget and P. L. F. Liu, 'Boundary calculations of sluice and spillway flows, *J. Hydraul. Div., Proc. ASCE*, **107**, (HY10), 1163–1178 (1981).
12. B. E. Larock and C. Taylor, 'Computing three-dimensional free surface flows', *Int. j. numer. methods eng.*, **10**, 1143–1152 (1976).
13. G. Mejak, 'Mixed boundary value problem for singular elliptic differential equation of second order', *IMFM Preprint Series*, **329**(29), (1991).
14. T. L. Labus and K. J. DeWitt, 'Liquid jet impingement normal to a disk in zero gravity', *J. Fluids Eng.*, **100**, 204–210 (1978).
15. T. N. Obee and K. J. DeWitt, 'Finite element analysis of free jet impingement', *Int. j. numer. methods eng.*, **15**, 63–85 (1980).
16. G. Hiriart and T. Sarpkaya, 'Finite element analysis of jet impingement on axisymmetric curved deflector, *Finite Elements in Fluids, Vol. 1*, Wiley, Chichester, 1975, pp. 265–279.
17. L. Trefethen, 'Surface tension in fluid mechanics', *Illustrated Experiments in Fluid Mechanics*, MIT Press, 1972. pp. 26–33.
18. J. C. Bruch and M. Dormiani, 'Free boundary fluid flow problems solved numerically in a hodograph plane using a fixed domain method', in C. Taylor *et al.* (eds), *Numerical Methods for Nonlinear Problems, Vol. 3*, Pineridge, Swansea, 1986, pp. 693–726.
19. R. W. Jeppson, 'Inverse formulation and FD solution for flow from a circular orifice', *J. Fluid. Mech.*, **40**, 215–223 (1970).
20. R. W. Jeppson, 'Inverse solution to three-dimensional potential flows', *J. Hydraul. Div., Proc. ASCE*, **98**, 789–812 (1972).
21. C. E. Pearson, 'Extension of a numerical streamline method', *Commun. Appl. Numer. Math.*, **1**, 177–181 (1985).
22. C. Cuvelier, 'On the computation of free boundaries', in P. Wesseling (ed.), *Research in Numerical Fluid Mechanics, Notes on Numerical Fluid Mechanics, Vol. 17*, Vieweg, Braunschweig, 1987.
23. H. Y. Lee and M. U. Kim, 'Numerical solution of plane and axially symmetric jet flow problems based on the variational inequality formulation, *Int. j. numer. methods fluids*, **10**, 213–222 (1990).
24. A. Acker, 'Convergence result for an analytical trial free boundary method', *IMA J. Numer. Anal.*, **8**, 357–364 (1988).
25. J. Serrin, 'Mathematical principles of classical fluid mechanics', in C. Trussdell (ed.), *Handbuch der Physik, Vol. VIII/1, Strömungsmechanik I*, Springer, Berlin, 1959.
26. P. Aubin, *Applied Functional Analysis*, Wiley, New York, 1979.
27. P. G. Ciarlet, *The Finite Element Method for Elliptic Problems*, North-Holland, Amsterdam, 1978.
28. J. W. H. Liu and A. H. Sherman, 'Comparative analysis of the Cuthill–McKee and reverse Cuthill–McKee ordering algorithms for sparse matrices', *SIAM J. Numer. Anal.*, **13**, 198–213 (1976).
29. W. Schach, 'Umlenkung eines kreisförmigen flüssigkeitsstrahles an einer ebenen platte senkrecht zur strömungsrichtung', *Ing. Arch.*, **6**, 51–59 (1935).
30. K. J. Bathe, *Finite Element Procedures in Engineering Analysis*, Prentice-Hall, Englewood Cliffs, NJ, 1982.
31. N. M. Schnurr, J. W. Williamson and J. W. Tatom, 'An analytical investigation of the impingement of jets on curved deflector', *AIAA J.*, **10**, 1430–1435 (1972).